Modelling the energy balance of acoustic emission

N. Pugno, G. Lacidogna, A. Carpinteri
Dipartimento di Ingegneria Strutturale e Geotecnica, Torino, Italy

F. Bosia
Dipartimento di Fisica, Politecnico di Torino, Torino, Italy

ABSTRACT: We present a simple mesoscopic model to describe the phenomenon of Acoustic Emission (AE) in a material undergoing damage in quasistatic tests. As in all damaging processes, in AE experiments a part of the mechanical energy stored in the deforming material is dissipated due to crack formation and propagation. The present model correctly accounts for energy dissipation due to the formation of micro-cracks and the creation of surfaces in the material as damage progression advances and is thus used to derive the AE scaling behaviour observed in experiments. A simple example is chosen to illustrate typical results obtained in numerical simulations using the model, namely a 2-D specimen in the form of a concrete bar subjected to uniaxial tests. The model is then used to fit data derived from experimental tests: first, on masonry elements of various sizes tested in compression by means of double flat-jacks; secondly, on a fibre-reinforced concrete specimen subjected to three-point bending. The numerical model presented here correctly reproduces the scaling behaviour and spatial distributions of AE events observed experimentally.

1 INTRODUCTION

Acoustic emissions (AEs) are caused by stress waves produced during the sudden internal stress redistribution from changes in the internal structure of a material subjected to loading (Carpinteri & Bocca 1991). Various attempts have been made in the literature to describe the qualitative and quantitative behaviour emerging from AE experiments (e.g. Turcotte 2003). Two-dimensional scalar lattice models for microfracturing have also been introduced, to numerically simulate the advancement of cracks and the resulting AE activity, including estimations of avalanche sizes and power-law behaviour (Zapperi, Vespignani & Stanley 1997). In most of the existing approaches, however, essential aspects of fracture mechanics are often neglected, such as energy dissipation and fracture energy balance.

Recent analysis of AE experiments has highlighted the multiscale aspect of cracking phenomena and fractal statistical analysis has been applied to describe the data (Carpinteri, Lacidogna & Pugno 2004). Energy dissipation has been shown to occur in a fractal domain comprised between a surface and a volume (Carpinteri & Pugno, 2005, Carpinteri, Lacidogna & Pugno, 2007). We aim at introducing these aspects in a simple numerical model that expands on the approaches appearing in the literature, and evaluating the influence of the proposed modifications on expected results. In particular, in this con-

tribution we model the experimental results obtained on masonry elements of various volumes, and verify the scaling behaviour obtained in the cumulative number of AE events generated in compressive tests with respect to specimen volume. Also, we consider three-point bending tests on fibre-reinforced concrete beams and use the model to simulate the experimentally derived spatial distribution of AE events.

2 MODEL

2.1 *Model description*

To correctly describe the phenomenon of AE in quasistatic experiments, our goal is to introduce the simplest possible model containing the correct energetic behaviour. For the sake of simplicity, we consider a specimen having length L_{tot} and cross-section A_{tot}. In a 2-D approximation, the specimen is modelled as a discrete arrangement of $N_x \times N_y$ springs, as shown in Figure 1. Each spring is identified by the index pair (i,j), with $i=1 \dots N_x$ and $j=1 \dots N_y$. The specimen is thus discretized in N_x portions, each modelled as an array of N_y parallel springs. Two opposite uniaxial forces of time-varying magnitude $F_{tot}(t)$ are applied at the two ends of the specimen, each undergoing a displacement of magnitude $x_{tot}(t)$ in the direction of the force. In the simplest possible approach, all springs are considered identical in

length l and in elastic parameters (Young's modulus E), but their cross-section A_{ij} is allowed to vary within chosen limits, i.e. $A_{min} < A_{ij} < A_{max}$, with the total specimen cross section remaining constant. The stiffness of a single spring can therefore be written as $k_{ij}=EA_{ij}/l$, whilst the equivalent stiffness of the i-th undamaged material portion, represented by the i-th arrangement of N_y parallel springs, is

$$K_i = \sum_{j=1}^{N_y} k_{ij} \tag{1}$$

The length and cross-section of the entire specimen are, respectively:

$$L_{tot} = \sum_{i=1}^{N_x} l_i = N_x l, \quad A_{tot} = \sum_{j=1}^{N_y} A_{ij} \ (\forall i) \tag{2}$$
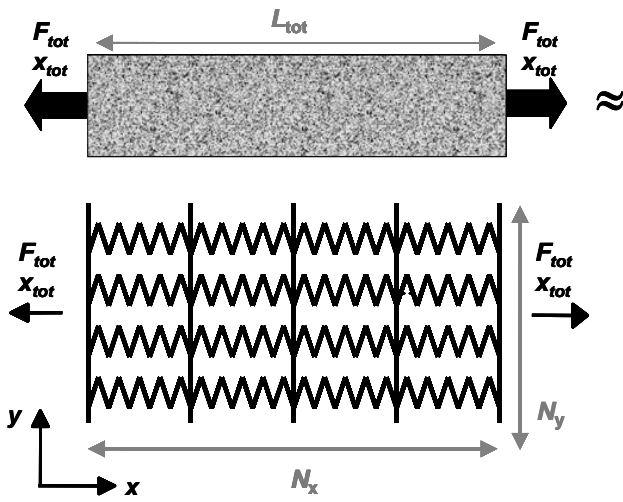

Figure 1. Discretization of a specimen subjected to uniaxial tension as adopted in simulations.

Next, we introduce a fracture criterion whereby the failure of the individual spring (i,j) occurs when it undergoes a stress σ_{ij} that exceeds its intrinsic strength σ_{Cij}. The value of σ_{Cij} is assumed to vary from spring to spring and to be distributed randomly, according to the Weibull distribution (Hermann & Roux 1990), which is widely used in fracture mechanics. The distribution $P(\sigma_{Cij})$ of the spring strengths can therefore be expressed as:

$$P(\sigma_{Cij}) = 1 - e^{\left[-\left(\frac{\sigma_{Cij}}{\sigma_C}\right)^m\right]} \tag{3}$$

where σ_C is a nominal stress value for the material under investigation, and m is the Weibull modulus, which is characteristic of the considered material. An AE event is modelled as the failure of a single spring used to discretize the specimen. In the case of failure of the (i,j)-th spring, its stiffness k_{ij} is set equal to zero. It is clear that, as the loading of the specimen increases and the resulting damaging process advances, the stiffness of each section of the material will decrease as fewer and fewer springs form-

ing the section remain intact. Therefore, the stiffness of each section is time dependent, i.e. $K_i = K_i(t)$. Correspondingly, the overall specimen compliance $C(t)$ increases in time. In particular, the overall specimen compliance variation $\Delta C(t)$ deriving from a single AE event occurring at the location (i,j) can be written as:

$$\Delta C_{ij}(t) = \frac{k_{ij}}{K_i(t)(K_i(t) - k_{ij})} \tag{4}$$

The denominator in Eq. (4) indicates that the variation ΔC_{ij} depends on time and on the location of the AE event taking place, as is intuitive.

We now turn our attention to the energetic aspects of AE events. Energy balance considerations require that the variation of the total potential energy $\Delta W_{ij}(t)$, when an AE event occurs, is compensated by the kinetic energy $\Delta T_{ij}(t)$ released in the form of a stress wave generated in the sample. The energetic contribution of the dissipated energy $\Delta \Omega_{ij}(t)$ in the formation of a crack surface at micro- or meso-scale must also be considered. Thus, we can write:

$$\Delta W_{ij}(t) + \Delta T_{ij}(t) + \Delta \Omega_{ij}(t) = 0 \tag{5}$$

The last term is important in order to obtain the correct scaling properties observed in AE experiments, as discussed below.

We further observe that in Force-Controlled (FC) or Displacement-Controlled (DC) quasistatic experiments the elastic potential energy variation for a spring failure (AE event) can be respectively written as:

$$(FC) \ \Delta W_{ij}(t) = -\frac{1}{2} F(t)^2 \Delta C_{ij}(t) \tag{6}$$

$$(DC) \ \Delta W_{ij}(t) = \frac{1}{2} x(t)^2 \Delta K_{ij}(t) \tag{7}$$

where $\Delta C(t)$ and $\Delta K(t)$ are the specimen compliance and stiffness variations, respectively, due to the AE event. The dissipated energy $\Delta \Omega$ is assumed to be proportional to the newly created surface A_{ij}:

$$\Delta \Omega_{ij} = G_C A_{ij} \tag{8}$$

where G_C is the critical strain energy release rate of the material. The above energy contributions can be expressed as a function of the accumulated elastic energy of the (i,j)-th spring at failure when the AE event takes place:

$$\Phi_{ij} = \frac{1}{2} \frac{\sigma_{Cij}^2}{E} A_{ij} l \tag{9}$$

In the case of quasistatic experiments, we can assume as a first approximation that, when a single spring used to discretize the specimen fails, the force acting on the corresponding specimen section will be redistributed evenly among all the adjacent springs. In this mean field approximation, the kinetic

energy released in AE can be written, according to the previous equations, as:

$$\Delta T_{ij}(t) = \left(\eta_i(t) - \gamma_{ij}\right)\Phi_{ij} \qquad (10)$$

where:

$$\gamma_{ij} = \frac{2EG_C}{\sigma_{Cij}^2 l} \qquad (11)$$

and

$$(FC)\ \eta_{ij}(t) = \frac{K_i(t)}{K_i(t) - k_{ij}}\ ; \qquad (12)$$

$$(DC)\ \eta_{ij}(t) = \frac{K(t+1)}{K(t)}\frac{K_i(t)}{K_i(t) - k_{ij}} \qquad (13)$$

with $K(t+1)$ and $K(t)$ the total specimen stiffnesses immediately before and after the AE event, respectively. The dissipated energy can also be expressed by means of the accumulated energy in the (i,j)-th spring:

$$\Delta\Omega_{ij} = \gamma_{ij}\Phi_{ij} \qquad (14)$$

2.2 Predictive capabilities

As an example, we consider a 2-D specimen in the form of a thin bar of length $L=10^{-2}$m and cross section $A_{tot}=10^{-6}$m^2, discretized by means of a $N_x=100$, $N_y=1000$ spring arrangement. The chosen material is concrete, with Young's modulus $E=23$GPa, peak stress $\sigma_C=10$ MPa, and Weibull modulus m varying between 1 and 6. To evaluate the influence of the variable spring cross section A_{ij}, two types of simulations are carried out: the first with all the springs having constant cross section ($A_{ij}=A_{tot}/N_y\ \forall i,j$), and the second by assigning random A_{ij} values, with the constraint that the specimen cross section remains constant ($\sum_j A_{ij} = A_{tot}$, $\forall i$).

Firstly, the specimen is subjected to traction with a displacement x_{tot} increasing linearly in time: $x_{tot}=vt$. We wish to compare the scaling properties for AE both when energy dissipation is accounted for and when it is not. The number of AE events, calculated without accounting for energy dissipation and indicated here with N_{AE}, correspond simply to the number of springs undergoing failure when their intrinsic strength is exceeded, whilst the released kinetic energy T accounts for energy dissipation, and is therefore a more realistic quantity to consider when comparing simulations to experiments.

We consider results for a typical numerical experiment with $m=3$, in the case of constant spring cross sections. The stress-strain curve displays only some softening before failure occurs. A less brittle behaviour can be obtained by choosing a small value

of N_x, whereby softening continues down to zero for increasing strain values.
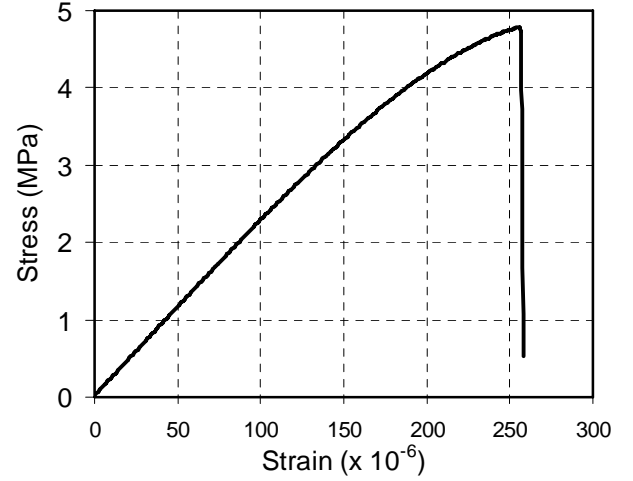

Figure 2. Stress-strain curve for a model specimen subjected to traction up to failure in a displacement-controlled simulation.

Typically, the number of AE events N_{AE} increases exponentially with time up to failure, as do the released kinetic energy T and the dissipated energy Ω. As discussed in detail elsewhere (Bosia, Pugno, Lacidogna & Carpinteri, 2007), it is possible to fit the data using a power law dependence, e.g. $N_{AE} \propto t^{\alpha}$, $T \propto t^{\beta}$ where α and β are non-integer exponents that are strongly dependent on the chosen Weibull modulus m. The simulated behaviour for T is shown in Figure 3. Best-fits are obtained for $\alpha = 2.7$ and $\beta = 6.8$ in this case. This fitting procedure supplies the possibility to compare predictions of specific experimental data.
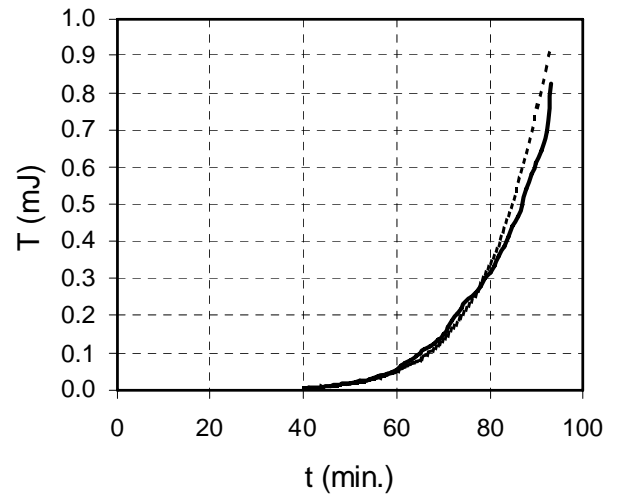

Figure 3. Exponential increase in the released AE kinetic energy T vs. time for a simulation with a linearly increasing displacement.

Our purpose is now to verify the predicted scaling behaviour with specimen dimensions (length, cross-section, and volume) and compare it with experimental results in the literature. Indeed, it was shown in experiments (Carpinteri, Lacidogna & Pugno, 2007) that the number of AE events scales with non-

integer exponents smaller than unity, indicating that AE occurs in a fractal domain with dimensions comprised between those of a surface and those of a volume. We therefore assume:

$$N_{AE}(L_{tot}) \propto L_{tot}^{d_{NL}}; \quad N_{AE}(A_{tot}) \propto A_{tot}^{d_{NA}}; \quad (15)$$

$$T(L_{tot}) \propto L_{tot}^{d_{TL}}; \quad T(A_{tot}) \propto A_{tot}^{d_{TA}} \quad (16)$$

and proceed to determine the relevant exponents d_{NL}, d_{NA}, d_{TL}, d_{TA} through simulations. To do this, specimens of different dimensions are considered. In particular, the specimen length L_{tot} is varied between 10^{-6}m and 10^{-2}m (with corresponding discretizations N_x varying between 1 and 1000) and the cross-section A_{tot} is varied between 10^{-10}m^2 and 10^{-4}m^2 (with corresponding discretizations N_y varying between 1 and 1000). Here, the results are discussed for constant spring cross-sections only.
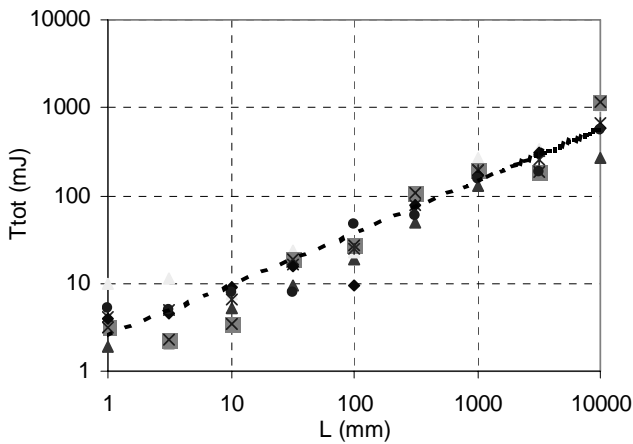

Figure 4. Numerically computed scaling properties of AE energy T vs. specimen length L_{tot} (plot in log-log scale).

As we are considering a uniaxial tensile test, we expect L_{tot} to be the relevant dimension with respect to which non-integer scaling occurs. Indeed, the exponents d_{NA}, d_{TA} are on average close to unity after repeated simulations, indicating direct proportionality with respect to specimen cross-section. On the other hand, simulations for different specimen lengths produce average values of $d_{NL}= 0.78$ and $d_{TL}= 0.57$, respectively. Both exponents are consistent with the experimentally derived effect of non-linear scaling. However, the latter of the two differs considerably from unity, indicating that the released kinetic energy in AE is a variable that displays the effect to a greater extent, and is possibly a better candidate for comparison with experimentally derived results. This is due to the fact that, when considering T instead of N_{AE}, the dissipated energy is accounted for, as explained above. Figure 4 displays typical results for the T vs. L_{tot} dependence in repeated numerical simulations.

Thus, despite its simplicity, the model seems to correctly reproduce a number of relevant experimentally observed characteristics of systems undergoing damage, including stress-strain curves and AE energy scaling versus specimen size.

3 MODELLING OF EXPERIMENTS

Experimental monitoring of damage progression has been carried out by some of the authors on various engineering structures, including historic buildings (Carpinteri, Lacidogna & Pugno, 2007). In order to support these tests and obtain information on the criticality of ongoing processes, measurements have also been carried out on single laboratory specimens in various loading configurations. Analysis of the scaling properties of these structures can then be used to assess the stability of the full-scale structures. Here, we show results from two of these laboratory tests, together with numerical predictions from the described model.

3.1 *Compressive tests on masonry elements*

First, a compressive test was conducted on three different masonry specimens through the combined use of double jacks and AE sensors. The prismatic masonry volumes tested in compression are shown in Figure 5.
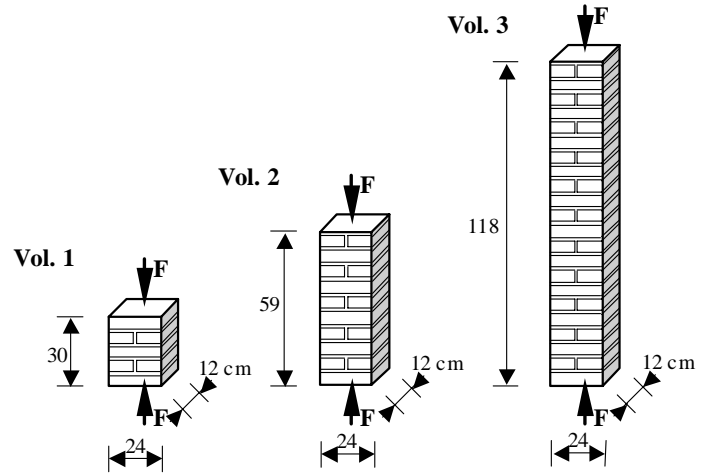

Figure 5. Masonry elements tested in compression by means of double flat-jacks (dimensions are expressed in cm). The bricks are 6 cm wide, while the mortar layers are 1 cm thick.

The dimensions of the cross-section of the elements correspond to the effective area of the masonry to which the pressure of the flat-jacks is applied. The tests comply with the procedures specified in ASTM 1991b, other than for the vertical cuts produced in order to eliminate, in the damaged element, the influence of the adjacent masonry portions.
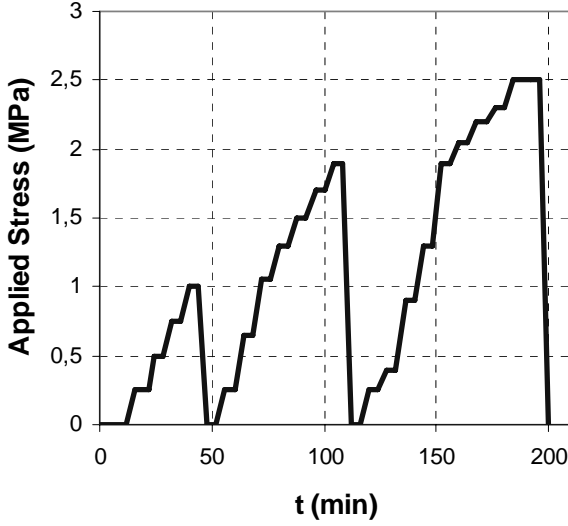
Figure 6. Adopted loading protocol in double flat-jack test on masonry elements.

Various loading cycles are applied with increasing stress levels, as shown in Figure 6, during which the cumulative number of AE events is monitored. For each test, the maximum number of AE events N_{max} at peak-stress is evaluated. Results are summarized in Table 1.

Table 1. Experimental values obtained from flat-jack tests and AE measurements

Specimen	Volume (cm^3)	Peak stress (MPa)	N_{max}
Vol. 1	8640	2.07	6500
Vol. 2	16992	1.61	12000
Vol. 3	33984	1.59	18000

3.1.1 *Simulations*
Simulations are carried out on the three specimens considered in experiments, with Young's modulus E=20 GPa, peak stress in compression σ_C=5 MPa, and critical strain energy release rate G_C =10 J/m^2. A 2-D discretization is used with 5000 elements in the length direction and 1000 elements in the width direction. The loading protocol shown in Figure 6 is applied in the simulations and the resulting cumulative number of AE events is recorded and compared to that obtained experimentally in each case. Good agreement is obtained in the three cases using Weibull modulus values comprised between 1.5 and 2. Results are shown in Figure 7 for the intermediate specimen (Vol. 2 in Figure 5). The plot shows that the material releases energy when the stress level reached previously is exceeded (Kaiser effect), a result obtained both experimentally and in simulations.

Again, we are interested in analysing the predicted scaling behaviour by varying specimen dimensions and comparing it with experimental results, to verify that AE indeed occurs in a fractal domain with dimensions comprised between those of a surface and those of a volume. Thus, we assume:

$$N_{AE}(V) \propto V^{D/3} \qquad (15)$$

where D is comprised between 2 and 3. Introducing the fractal acoustic emission density Γ_{AE}, we can write:

$$\Gamma_{AE} = N_{max}/V^{D/3} \qquad (16)$$

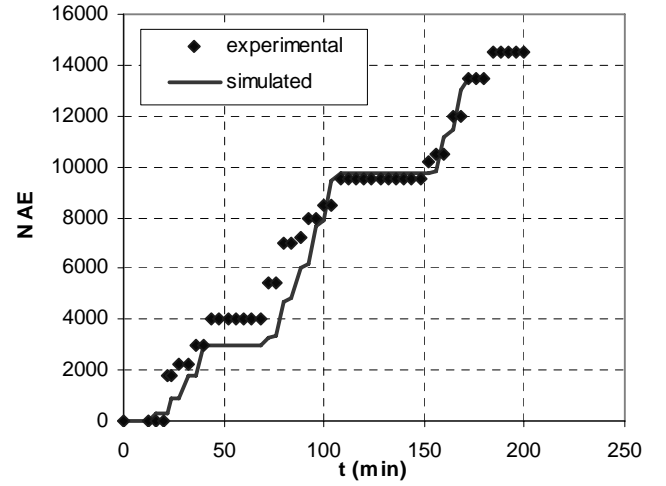where N_{max} is the maximum number of AE events, evaluated at peak-stress.

Figure 7. Simulated and experimental number of AE events vs. time for Vol. 2, using the loading protocol in Figure 6.

The experimental results summarized in Table 1 show that the cumulative number of AE events increases nonlinearly with increasing specimen volume. By best-fitting of the results of these tests, we obtain $D/3 \cong 0.743$, so that the fractal exponent, as predicted by fragmentation theories, turns out to be $D \cong 2.23$, and the critical value of fractal AE density $\Gamma_{AE} \cong 8.00$ cm$^{-2.23}$.
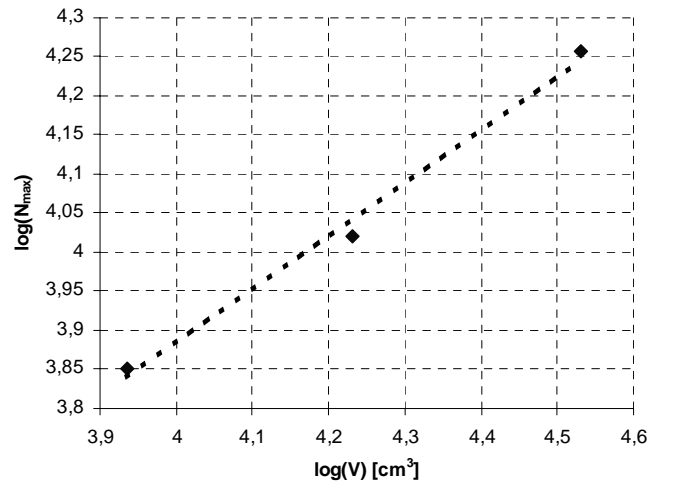

Figure 8. Simulated AE scaling behaviour (dots) by varying the specimen volume. A linear fit (dotted line) on the data (dots) yields the value $D = 2.05$.

Numerical simulation results for scaling of N_{AE} vs. specimen volume V are shown in Figure 8. Similar values to those obtained experimentally are derived, and fitting of the data yields a fractal exponent of $D\cong2.05$, slightly below the experimental value ($D\cong2.23$). The value obtained numerically for the fractal exponent D when one considers the total released kinetic energy T instead of N_{AE} is comparable. However, from a physical point of view, T is a better candidate for comparison with experimental results, due to the fact that in the latter case the dissipated energy in surface formation is accounted for.

3.2 *Three-point bending of a FRC beam*

As a second example, we consider a $100\times15\times15$ cm^3 fibre-reinforced concrete (FRC) beam loaded up to failure according to the three-point bending test geometry and subjected to AE monitoring. The beam has a central notch 5 cm long with a fibre content of 40 kg/m^3 for a resulting Young's modulus of 35 GPa. The simulations are performed in displacement control by imposing a constant displacement rate equal to 10^{-3} mm/s.

3.2.1 *Simulations*
The specimen is modelled by adopting a 2-D discretization, and by applying the analytically calculated bending stresses to each material portion at every time step. An AE event is generated whenever the applied stress locally exceeds the assigned peak stress. Each AE event implies the reduction of the local moment of inertia and of the local stiffness in correspondence with the cross-section where the event is generated, i.e. portions of the material where numerous fracture events have occurred will experience greater stresses and are thus more likely to fail.

Simulations are carried out of a 2-D specimen of dimensions $85\times15\times15$ cm^3 (the specimen portion subjected to bending stresses), Young's modulus $E=35$ GPa, peak stress $\sigma_C= 45$ MPa (both in traction and in compression), and critical strain energy release rate $G_C =10$ J/m^2. The specimen is discretized by using 3400×600 elements (in the x and y directions, respectively). Fracture maps of the damaged specimen are calculated at failure. Results coincide to a great extent to those obtained experimentally, both in the spatial distribution of the fractures and in their distribution of occurrence in time. The AE events take place mainly in the central section of the specimen, close to the notch, and towards the upper and lower boundaries of the specimen, where tensile and compressive stresses are the greatest. The extent to which the simulated AE sources concentrate around the notch is mainly dependent on the chosen Weibull modulus m for simulations. Thus, the spatial distribution of AE events is another quantity that allows the verification of the validity of the model,

and guides towards an appropriate choice of material parameters. Figure 9 illustrates typical results for $m=3$.
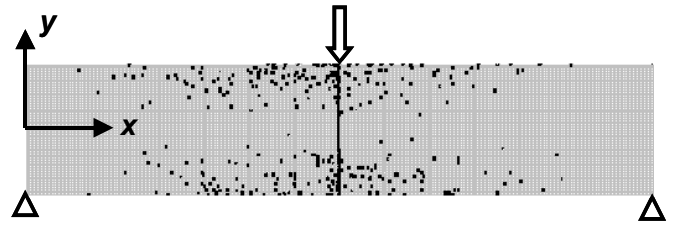

Figure 9. Damage localization in a simulated 3-point bending experiment up to failure. Dark regions indicate the locations of AE events.

4 CONCLUSIONS

We have presented a simple phenomenological model that allows us to capture a number of important characteristics that emerge in damage progression experiments and AE measurements. In particular, the power law scaling behaviour with respect to specimen volume obtained experimentally in tests on masonry elements is correctly reproduced, as is the experimental spatial distribution of AE events in a FRC beam subjected to three-point bending. Having verified the reliability of the model, its predictive possibilities will be further investigated in the case of different materials and experimental configurations.

REFERENCES

Bosia F., Pugno N., Lacidogna G., Carpinteri A. Iin preparation.

Carpinteri A., Bocca P. 1991 In *Damage and Diagnosis of Materials and Structures*, Ed. Pitagora (Bologna).

Carpinteri A., Lacidogna G., Pugno N., 2004. Damage diagnosis and life-time assessment of concrete and masonry structures by an acoustic emission technique, in V.C. Li et al. (eds.), *Fracture Mechanics of Concrete and Concrete Structures (Proceedings of the 5th International FraMCoS Conference, Vail, Colorado, USA)* 1: 31- 40.

Carpinteri A., Pugno N.,. 2005. Are scaling laws on strength of solids related to mechanics or to geometry? *Nature Materials* 4 (6): 421-423.

Carpinteri A., Lacidogna G., Pugno N., 2007. Structural damage diagnosis and life-time assessment by acoustic emission monitoring. *Eng. Frac. Mat.* 74: 273-289.

Hermann, H.J. & Roux, S. 1990. Modelization of fracture in disordered systems. In H.J.Hermann & S.Roux (eds.), *Statistical Models for the Fracture of Disordered Media*. North Holland: Elsevier Science publishers.

Turcotte, D.L. 2003. Micro and macroscopic models of rock fracture. *Geophys. J. Int* 152: 718-728.

Zapperi S., Vespignani A., Stanley, H.E. 1997. Plasticity and avalanche behaviour in microfracturing phenomena. *Nature* 388: 658-660.